mater.scichina.com link.springer.com

Published online 27 September 2022 | https://doi.org/10.1007/s40843-022-2210-9
Sci China Mater 2023, 66(2): 733–739

Directed self-assembly of organic crystals into chip-like heterostructures for signal processing

Chao-Fei Xu[1†], Wan-Ying Yang[1†], Qiang Lv[1], Xue-Dong Wang[1*] and Liang-Sheng Liao[1,2*]

ABSTRACT **Organic single crystals show broad application prospects in the field of optical confinement and waveguides due to their low optical transmission loss and tunable optical properties. Individual one- or two-dimensional (1D or 2D) optical waveguide crystals have the limitations of a single function in organic photonics. In this work, a chip-like organic heterostructure was fabricated using an elaborately designed, sequential growth method. By regulating the concentration of each organic component, the processes of solution self-assembly, etching, and epitaxial self-assembly are successively performed to complete the directional growth of organic micro/nanostructures. Notably, the as-prepared chip-like organic heterostructure is composed of 1D/2D optical waveguide crystals, which can realize multidimensional photon transportation and multi-terminal directional optical signal output. Furthermore, the unique 2D optical waveguide properties of the chip-like heterostructures offer opportunities for constructing the encoding form of the output optical signal at the micro/nanoscale.**

Keywords: organic crystal, heterostructure, optical waveguide, solution self-assembly, on-chip photo-processing

INTRODUCTION

With the rapid development of science and technology, the demand for bandwidth and information density in the fields of information and communication technology, computing, and storage is increasing day by day [1]. The development of traditional integrated electronic systems with electrons as the carrier has encountered the bottleneck of size and energy consumption [2]. As an information transmission medium, photons have the advantages of high speed, low energy consumption, and low noise compared with electrons [3]. Therefore, as a promising solution for future massive data transmission and processing, optoelectronic composite integrated systems have received more attention [4,5], with the focus on preparing basic materials and exploring feasible strategies [6–8].

Generally, organic micro/nanocrystals are candidate basic materials for optoelectronic integrated systems because of their unique optoelectronic properties and excellent tunable optical waveguide properties [9,10]. Many potentially feasible strategies and ideas have been proposed for preparing different structures with crystalline materials, including microrods and microsheets that can be used for light propagation [11,12]. Microrod is a typical one-dimensional (1D) optical waveguide material that ensures unidirectionality during optical signal propagation. Many homostructures and heterostructures based on microrods have been developed, such as the core-shell [13,14], block [15,16], and branch [17,18] types, enabling a variety of unique optical applications [19,20]. The 2D optical waveguide materials, mainly based on micron chips, can transmit optical signals in multiple directions, realize more complex optical waveguide functions, and are more suitable for on-chip photonic integrated systems [21,22]. However, single microrods or microsheets have application limitations, so increasingly more studies seek to combine these two structures to construct more complex and diverse heterostructures to explore materials and strategies for photonic integrated systems [23,24].

In this work, we report the fabrication strategy and potential photonic integration applications of complex, chip-like heterostructures comprising a microsheet of benzo[*ghi*]perylene (BGP) and multiple microrods of BGP/3,4,5,6-tetrafluorophthalonitrile (*o*-TFP) cocrystal. The heterostructures are prepared by the sequential growth process. The growth order of the crystal structure is well controlled through regulating different component concentrations. Then, introducing the key micro-etching process creates conditions for the epitaxial growth of microrods. Under the action of the lattice matching mechanism, the regular chip-like heterostructures are finally fabricated. The optical property test of the heterostructure shows that, on the basis of the optical waveguide properties of the two components, chip-like heterostructures combine the modulability of the light source and the directionality of the output, which guarantees its application for on-chip photonic modulation. Furthermore, the unique optical waveguide properties of chip heterostructures also give us inspiration and opportunities to propose modulation and coding schemes for output optical signals. The fabricated, chip-like heterostructures propose feasible structural prototypes for on-chip photo-processing, demonstrating their promising applications in the field of photonic integration. The preparation method of the sequential growth process also provides a designable strategy for building the infrastructure of

[1] Institute of Functional Nano & Soft Materials, Jiangsu Key Laboratory for Carbon-Based Functional Materials & Devices, Soochow University, Suzhou 215123, China
[2] Macao Institute of Materials Science and Engineering, Macau University of Science and Technology, Taipa 999078, Macao, China
[†] These authors contributed equally to this work.
[*] Corresponding authors (emails: wangxuedong@suda.edu.cn (Wang XD); lsliao@suda.edu.cn (Liao LS))

photonic integrated systems.

RESULTS AND DISCUSSION

Preparation and characterization of organic chip-like heterostructures

As shown in Fig. 1a, chip-like heterostructures that can be used for multi-terminal optical signal output and modulation are prepared by combining BGP microsheets and BGP/*o*-TFP cocrystal microrods *via* a sequential growth process. The bi-directional π-π stacking makes the BGP molecules self-assemble into the microsheet crystals, as shown in Fig. 1b. Under ultraviolet (UV) lamp excitation, the BGP microsheets exhibit green luminescence confirmed by the spectral data (Fig. S1, red line). The microsheets exhibit bright pale green formed by the intermolecular charge transfer (CT) between the donor molecule BGP and the acceptor molecule *o*-TFP (Fig. 1c). Different fluorescence lifetimes at room temperature reveal the formation of the cocrystal (Fig. S2). When combined into heterostructures, microsheets and microrods retain the original characteristics of single crystals, and the cocrystal microrods are evenly distributed around the BGP microsheets (Fig. 1d). For comparison, cocrystals of BGP with different receptors (*m*-TFP or *p*-TFP) were also prepared and extended to the preparation of heterostructures (Figs S3 and S4). The different energy gaps between the donor molecule and different acceptor molecules are the main reason for the change in the emission spectra and diffuse reflectance absorption spectroscopy of the cocrystals (Figs S1 and S5). In addition, to explore the possibility of different structures, a metastable heterostructure based on the BGP donor-acceptor system was prepared in the mixed solvent ($V_{dichloromethane}/V_{ethanol}$ = 1:1.5) (Fig. S6). Generally, such chip-like heterostructures combine the characteristics of the two single crystals, exhibit unique optical properties, and have potential optical integration applications, such as optical signal coupling transmission and optical signal modulation.

Mechanism of the directed self-assembly of organic crystals into chip-like heterostructures

Chip-like heterostructures were fabricated through an elaborately designed sequential growth process. A video was taken in a bright field to record the actual growth process of the heterostructure, and the main content of the video is shown in Fig. 2a$_1$–a$_{10}$. According to different phenomena of crystal growth, the heterostructure formation can be divided into three stages. In the first stage, from 0 to 68 s, by controlling the concentration of different components, BGP molecules nucleated first and assembled into microsheets. In the second stage (68–103 s), the microsheets grew larger, and micro-etching appeared on the surface. Finally, with the evaporation of the solvent, the cocrystal microrods quickly grew epitaxially around the microsheets, forming the heterostructures (103–224 s).

A series of test experiments and theoretical calculations were performed to reveal the growth mechanism of the heterostructures. A schematic diagram drawn in Fig. 2b visually presents the mechanistic explanation for each stage of the sequential growth process. In general, cocrystal systems with strong intermolecular interactions preferentially nucleate, favoring the

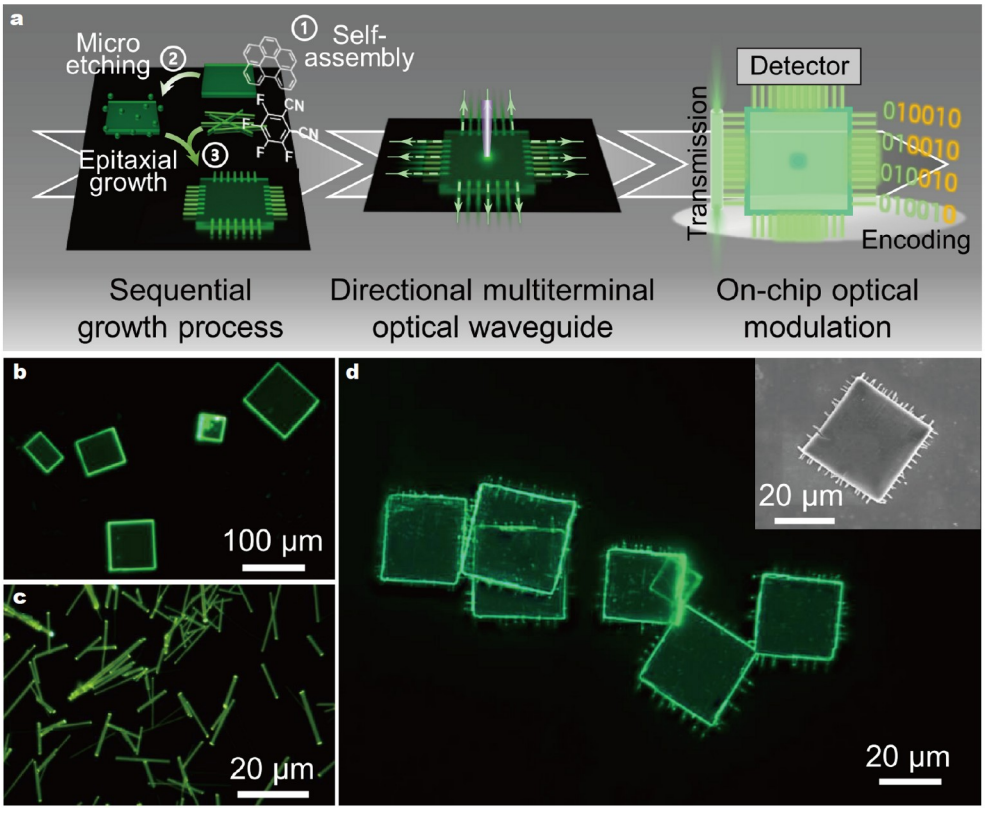

Figure 1 (a) Main research content and process of the fabrication of the organic chip-like heterostructures. Photoluminescence (PL) microscopy image of the green-emitting BGP microsheets (b), the yellow-green-emitting BGP/*o*-TFP cocrystal microrods (c) and the chip-like heterostructures (d) under the excitation of unfocused UV light from a xenon lamp. Inset of (d): scanning electron microscopy (SEM) image of a typical chip-like heterostructure.

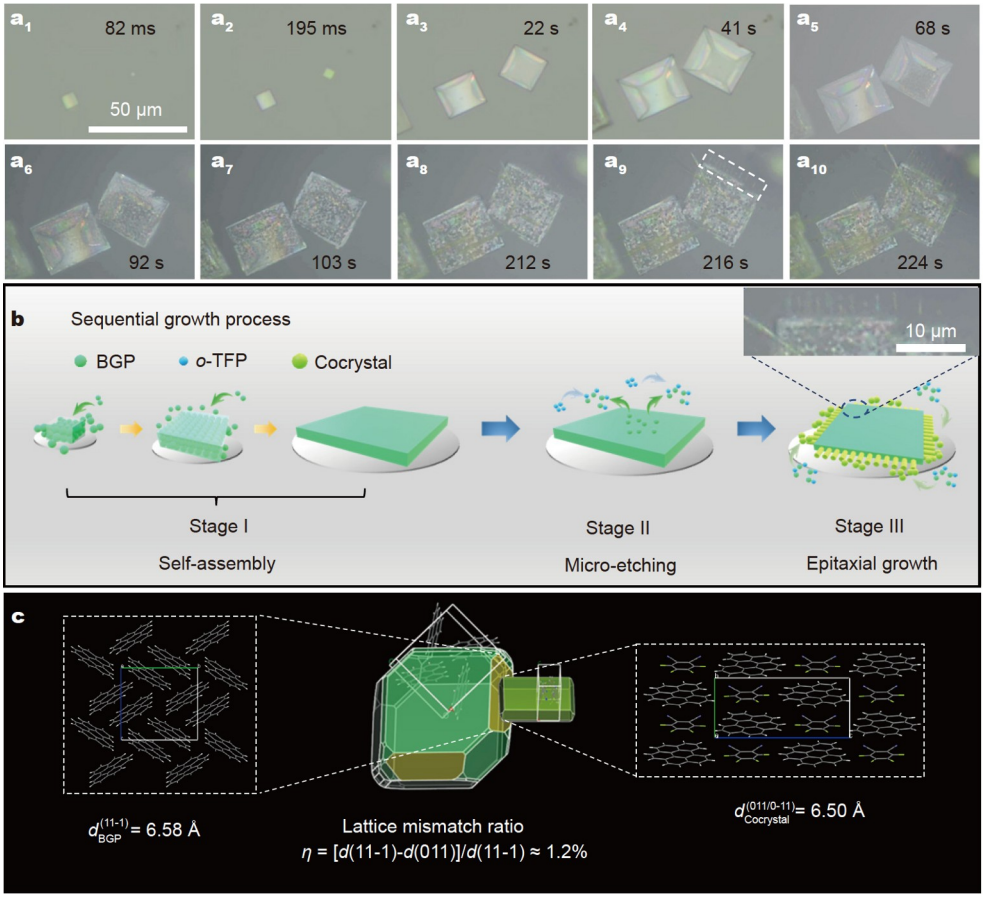

Figure 2 (a_1–a_{10}) Growth process of the chip-like heterostructures. The scale bars are 50 μm. The fabrication of heterostructures was accomplished in a mixed solvent system with a ratio of $V_{dichloromethane}/V_{ethanol}$ = 1:1. (b) Schematic diagram of the growth mechanism of the chip-like heterostructures. The top right inset is an enlarged view of the portion marked by the dotted box in (a_9). The scale bar is 10 μm. (c) The lattice matching between BGP microsheets and BGP/*o*-TFP cocrystal microrods. η is the lattice mismatch ratio between the crystal planes.

sequential self-assembly of heterostructures [25–27]. Theoretical calculation results (Table S1) show that the π-π interaction (−18.53 kcal mol^{-1}) between BGP molecules is similar to the CT interaction (−16.75 kcal mol^{-1}) between BGP/*o*-TFP, which means that BGP single crystal microsheets and cocrystal microrods will be formed almost simultaneously. The sequence of crystal nucleation and crystallization is also affected by other factors, such as saturated solubility and system energy [28]. According to the Beer-Lambert law, the saturated solubility of BGP and *o*-TFP in dichloromethane (DCM) and DCM/ethanol (DCM/EtOH) mixed solution was calibrated by testing the absorbance of different concentration solutions and saturated solutions (Table S2). The saturated solubility of BGP in DCM and the mixed solution is much less than that of *o*-TFP, so BGP precipitates and nucleates more easily from the mixed solution than *o*-TFP. Moreover, during the transformation from a single-molecule state into a crystal, the energy reduction of the first nucleated crystallization system is larger than that of the later nucleated crystallization system [29,30]. Theoretical calculations (Table S1) show that the system energy reduction caused by forming a BGP single crystal is −33.55 kJ mol^{-1}, and the system energy reduction caused by forming the BGP/*o*-TFP cocrystal is −314.64 kJ mol^{-1}, which explains why BGP single crystal microsheets are formed first.

The schematic diagram in Fig. 2b visually presents the mechanistic explanation for each stage of the sequential growth process. When the BGP crystals gradually grow into stable microsheets, many *o*-TFP molecules remain in the solution. Because of the CT force between the donor and the acceptor, the remaining *o*-TFP molecules in the solution combine with the BGP molecules on the surface of the microsheets, causing them to be released from the crystals. This process forms a weak etching on the surface of the microsheets. The BGP molecules detached from the microsheets redissolve into the solution and nucleate with the *o*-TFP molecules as cocrystals. This top-down etching process results in the formation of a few defects on the surface of the microchip, which provide sites and substrates for the epitaxial growth of cocrystal microrods. With the continuous volatilization of the solution, the BGP/*o*-TFP donor-acceptor combination finally nucleated and crystallized as cocrystal microrods. Finally, as shown in the inset of Fig. 2c, because of the inherent lattice matching between the (11−1) crystal planes of the BGP microsheets and the (011/0−11) crystal planes of the cocrystal microrods, the microrods can be epitaxially grown uniformly around the microsheets.

Applications for optical signal processing and directional output

Spatially resolved PL spectra tests were implemented to study the optical waveguide performance of the single crystals and heterostructures. The results are consistent with previous experi-

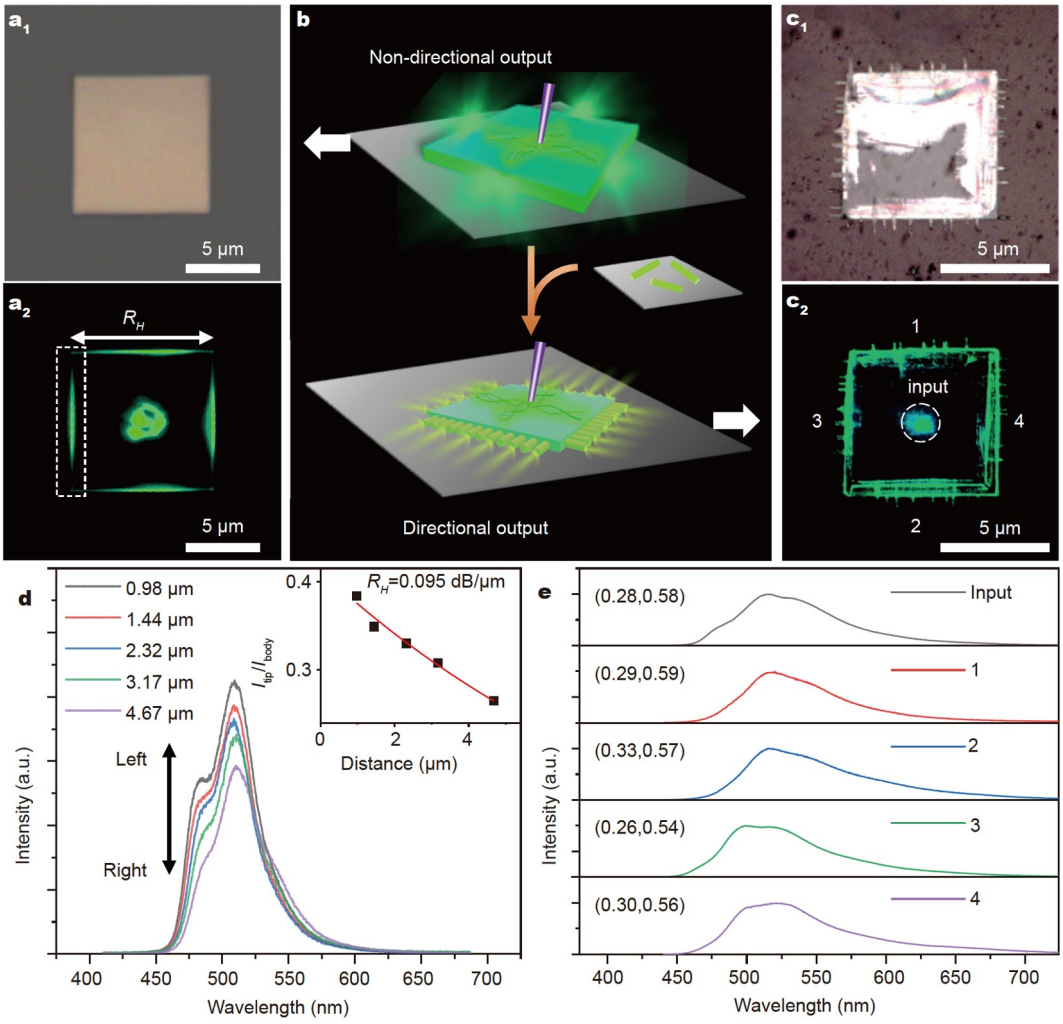

Figure 3 (a_1) Bright-field microscopy image of a typical BGP microsheet. (a_2) PL microscopy image of the same BGP microsheet under the excitation of a 375-nm laser beam. The scale bars are 5 μm. (b) Different forms of 2D optical signaling of single BGP microsheets and chip-like heterostructures. (c_1) Bright-field microscopy image of a typical chip-like heterostructure. (c_2) PL microscopy image of the same heterostructure under the excitation of a 375-nm laser beam. The scale bars are 5 μm. (d) Spatially resolved PL spectra of the BGP microsheet in (c) with the excitation point moving horizontally. Inset: ratio between the I_{tip}/I_{body} *versus* the distance X at 510 nm. (e) Micro-area spectral signals collected from the excitation point and the microrod output terminal at four edges.

ence, indicating that BGP microchips are a good 2D optical waveguide material [21,31]. Fig. 3a shows that, under the excitation of a 375-nm laser beam, the microsheet produces 520nm green light, which propagates in multiple directions from the excitation point to the edge. As the laser beam moves horizontally or longitudinally on the microsheet in the direction of the arrow, the corresponding spatially resolved spectra from the edges of the microchip are collected (Fig. 3d and Fig. S7b). Then, the correlation curve between the ratio (I_{edge}/I_{body}) and the propagation distance at 520 nm obtained by nonlinear fitting is given in the upper right inset of Fig. 3d. The optical loss coefficients (R) of the BGP microsheets in the horizontal direction (R_H = 0.095 dB μm^{-1}) and longitudinal direction (R_L = 0.116 dB μm^{-1}) are calculated by the single exponential nonlinear attenuation function of $I_{edge}/I_{body} = A\exp(-RX)$, where X represents the distance between the excitation point and the edge marked by the dashed box [32]. Tiny and uniform waveguide losses suggest that the microsheet is a good light source and optical transmission medium. The change in the light signal intensity from the edge caused by moving the excitation position reflects the light modulation property of the microsheet, which indicates that the microchip is suitable as the basic structure for on-chip light processing. Similar tests were also performed on BGP/*o*-TFP cocrystal microrods. A typical cocrystal microrod is locally excited by a 375-nm laser beam, and the excited optical signal transmits from the excitation point along the microrod and finally outputs from the tips, showing the characteristics of a 1D optical waveguide (Fig. S8) [33]. Obviously, microsheets and microrods have different optical waveguide properties and have their own limitations [34].

The desired tunable 2D optical waveguide can be realized by microsheets, but it is also noticed that due to the divergence of light propagating on the microsheets, the microchips face the problem of light output non-directionality in further light processing applications (Fig. 3b, top schematic diagram). In contrast, although microrods can only realize a single-direction optical waveguide along the growth direction, this waveguide ensures the concentration and directionality of the signal. The

prepared chip-like heterostructure is advantageous because the two basic optical waveguide modes are combined by integrating cocrystal microrods around the microsheet, which effectively compensates for the application shortcoming of a single crystal and realizes multi-terminal directional output of optical signals (Fig. 3b, bottom schematic diagram). Further research on the optical properties of heterostructures was conducted by testing the output optical signal from the terminals. When a typical chip-like heterostructure is excited with a 375-nm laser beam, as shown in Fig. 3c, the light propagates from the excitation point to the edge of the microsheet in multiple directions and then is output directionally by the microrod. Optical signals can be detected at the microrod terminals around the heterostructure, and the corresponding spectra are also recorded, as shown in Fig. 3e. The wavelength of the signal ranges from approximately 450 nm to approximately 650 nm, which is basically consistent with the emission wavelength range of the BGP microplates and cocrystal microrods. The similar luminescence of the microsheet and the microrod ensures the uniformity of the optical signal and simultaneously reduces the optical loss caused by self-absorption. Because of the integration of the microrods, the heterostructure solves the problems that a single microplate would face in light processing applications and enables more complex light modulation.

Modulatable on-chip optical signal coding scheme

The microrod ensures the directionality of the optical signal output from the heterostructure, and the microsheet as the light

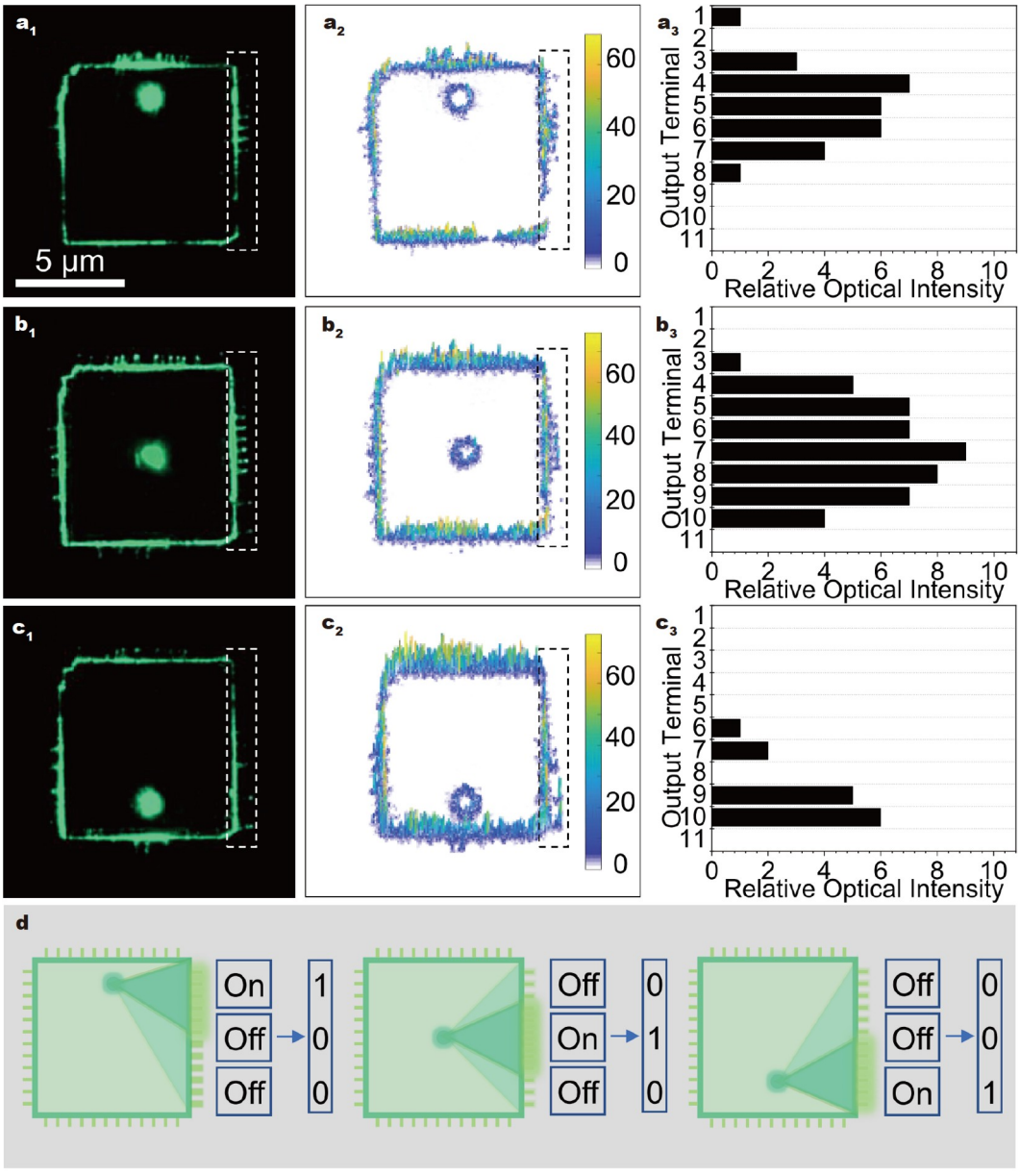

Figure 4 (a_1–c_1) PL microscopy images of a typical chip-like heterostructure. The scale bars are 5 μm. (a_2–c_2) Optical signal intensities of the heterostructures under the excitation of a 375-nm laser beam at three positions extracted by Matlab software. (a_3–c_3) Histograms of the relative value of the optical signal intensity of the output terminals on the right side of the heterostructure marked by the dashed box. (d) Schematic diagram of digital signal encoding-based on-chip-like heterostructure multi-terminal signal output.

Table 1 Coding results corresponding to the light signal transmission of the chip-like heterostructure when the excitation point is in nine main typical positions. The coding order is from left to right and from top to bottom

Pattern	Code	Pattern	Code	Pattern	Code
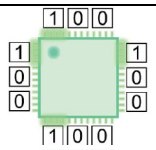	100 100 100 100	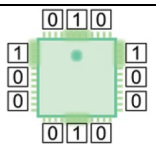	010 100 100 010	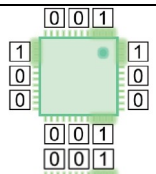	001 100 100 001
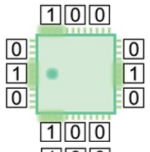	100 010 010 100	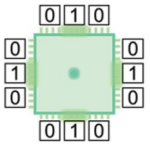	010 010 010 010	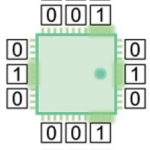	001 010 010 001
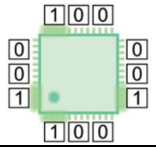	100 001 001 100	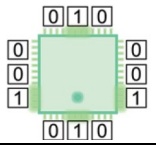	010 001 001 010	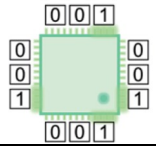	001 001 001 001

source and the pre-transmission medium ensures the modulability of the light source, which provides a structural basis for the on-chip optical processing of the heterostructure. To further study and analyze the optical application of the heterostructures, we changed the position of the excitation point on the heterostructures through spatially resolved microscopy (Fig. 4a$_1$–c$_1$). Then, we recorded the signal transmission phenomena in different situations and extracted the relative light intensities of different microrod output terminals of the heterostructures using Matlab software. In Fig. 4a$_2$–c$_2$, the peak stereogram corresponding to the optical signal intensity is constructed; the height and color of the peak represent the intensity of the light signal. As the position of the excitation point moves, the intensity of the optical signal at the output changes accordingly. To intuitively and quantitatively understand this change, the corresponding histograms are plotted as shown in Fig. 4a$_3$–c$_3$. Taking the output port on the right side of the heterostructure as an example, the relative optical signal intensity bar chart was drawn. We specify that the maximum optical signal intensity is 10 and the minimum is 1, and the length of the column represents the optical signal intensity of each output port. From this specification, we can see that the optical signal intensity of different output terminals is directly related to the position of the excitation point. The optical signal intensity of the output port within the same level range as the excitation point is larger, and those of the other output ports are weaker. In other words, by simply changing the position of the excitation point, we can control the switch of the output optical signal from different terminals. Thus, the chip-mounted heterostructure is an optical modulation model with controllable switchable multi-terminal signal directional output, which creates conditions and inspirations for optical signal encoding. Therefore, on the basis of a multi-terminal switch controlled by the excitation position change, we propose a modulation coding scheme for the output optical signal. According to the bar chart, we specify that the terminal whose relative signal strength is lower than 5 corresponds to code "0", and the port whose relative signal strength is greater than 5 is code "1". As shown in Fig. 4d, taking the port on the right as an example, the signal strength varies correspondingly with the location of the excitation point, and the combination of codes varies. When the excitation point is in the upper center, the upper port has a stronger signal, and the middle and lower ports have a weaker signal. By definition, the code combination is "100". When the excitation point moves to the center or lower center position, the corresponding code combinations are "010" and "001", respectively. According to this rule, the code combinations corresponding to the ports of other edges can also be obtained. Furthermore, when the excitation points are located in nine special positions, more complex codes can be obtained corresponding to all the ports of the four edges (Table 1). Therefore, combining multi-terminal optical signal output and modulation into complex digital signals provides a feasible solution for the future integrated photonics system.

CONCLUSIONS

The chip-like heterostructure prepared by integrating BGP microsheets and BGP/*o*-TFP cocrystal microrods has the modulability of the light source and realizes the multi-terminal directional output of optical signals. Based on the unique optical transmission properties of the heterostructures, we developed the function of a multi-terminal optical signal switch and proposed a scheme for the modulation and coding of an output optical signal. The properties and functions of the chip-mounted heterostructures are an indispensable part of on-chip optical processing, providing a structural basis for constructing photonic integrated systems. The ingeniously designed sequential growth preparation method and the practice of the modulation and coding of optical signals based on-chip-like heterostructures shed light on developing on-chip optical processing and photonic integration.

Received 31 May 2022; accepted 28 July 2022; published online 27 September 2022

1 Clark J, Lanzani G. Organic photonics for communications. Nat Photon, 2010, 4: 438–446
2 Ning CZ. Semiconductor nanolasers and the size-energy-efficiency challenge: A review. Adv Photon, 2019, 1: 1
3 Kim JH, Aghaeimeibodi S, Carolan J, *et al.* Hybrid integration methods for on-chip quantum photonics. Optica, 2020, 7: 291–308
4 An J, Zhao X, Zhang Y, *et al.* Perspectives of 2D materials for optoelectronic integration. Adv Funct Mater, 2022, 32: 2110119
5 Bogaerts W, Pérez D, Capmany J, *et al.* Programmable photonic circuits. Nature, 2020, 586: 207–216

6 Chen M, Lu L, Yu H, *et al.* Integration of colloidal quantum dots with photonic structures for optoelectronic and optical devices. Adv Sci, 2021, 8: 2101560
7 Liu J, Qu J, Kirchartz T, *et al.* Optoelectronic devices based on the integration of halide perovskites with silicon-based materials. J Mater Chem A, 2021, 9: 20919–20940
8 Ma S, Zhou K, Hu M, *et al.* Integrating efficient optical gain in high-mobility organic semiconductors for multifunctional optoelectronic applications. Adv Funct Mater, 2018, 28: 1802454
9 Wang C, Dong H, Jiang L, *et al.* Organic semiconductor crystals. Chem Soc Rev, 2018, 47: 422–500
10 Ito S. Luminescent polymorphic crystals: Mechanoresponsive and multicolor-emissive properties. CrystEngComm, 2022, 24: 1112–1126
11 Shi Y, Wang X. 1D organic micro/nanostructures for photonics. Adv Funct Mater, 2020, 31: 2008149
12 Shi YL, Zhuo MP, Wang XD, *et al.* Two-dimensional organic semiconductor crystals for photonics applications. ACS Appl Nano Mater, 2020, 3: 1080–1097
13 Zhuo MP, Wang XD, Liao LS. Construction and optoelectronic applications of organic core/shell micro/nanostructures. Mater Horiz, 2020, 7: 3161–3175
14 Yu Y, Tao YC, Zou SN, *et al.* Organic heterostructures composed of one- and two-dimensional polymorphs for photonic applications. Sci China Chem, 2020, 63: 1477–1482
15 Zhuo MP, Wu JJ, Wang XD, *et al.* Hierarchical self-assembly of organic heterostructure nanowires. Nat Commun, 2019, 10: 3839
16 Wang K, Zhang W, Gao Z, *et al.* Stimulated emission-controlled photonic transistor on a single organic triblock nanowire. J Am Chem Soc, 2018, 140: 13147–13150
17 Li ZZ, Tao YC, Wang XD, *et al.* Organic nanophotonics: Self-assembled single-crystalline homo-/heterostructures for optical waveguides. ACS Photonics, 2018, 5: 3763–3771
18 Ma YX, Wei GQ, Chen S, *et al.* Self-assembled organic homostructures with tunable optical waveguides fabricated *via* "cocrystal engineering". Chem Commun, 2021, 57: 11803–11806
19 Cao J, Liu H, Zhang H. An optical waveguiding organic crystal with phase-dependent elasticity and thermoplasticity over wide temperature ranges. CCS Chem, 2021, 3: 2569–2575
20 Bao Q, Goh BM, Yan B, *et al.* Polarized emission and optical waveguide in crystalline perylene diimide microwires. Adv Mater, 2010, 22: 3661–3666
21 Liu Y, Hu H, Xu L, *et al.* Orientation-controlled 2D anisotropic and isotropic photon transport in co-crystal polymorph microplates. Angew Chem Int Ed, 2020, 59: 4456–4463
22 Dong H, Zhang C, Shu FJ, *et al.* Superkinetic growth of oval organic semiconductor microcrystals for chaotic lasing. Adv Mater, 2021, 33: 2100484
23 Chen S, Yin H, Wu JJ, *et al.* Organic halogen-bonded co-crystals for optoelectronic applications. Sci China Mater, 2020, 63: 1613–1630
24 Han S, Zhang W, Qiu B, *et al.* Controlled assembly of organic composite microdisk/microwire heterostructures for output coupling of dual-color lasers. Adv Opt Mater, 2018, 6: 1701077
25 Lv Q, Wang XD, Yu Y, *et al.* Lattice-mismatch-free growth of organic heterostructure nanowires from cocrystals to alloys. Nat Commun, 2022, 13: 3099
26 Zhuo MP, Su Y, Qu YK, *et al.* Hierarchical self-assembly of organic core/multi-shell microwires for trichromatic white-light sources. Adv Mater, 2021, 33: 2102719
27 Tan C, Chen J, Wu XJ, *et al.* Epitaxial growth of hybrid nanostructures. Nat Rev Mater, 2018, 3: 17089
28 Chen S, Wang X, Zhuo M, *et al.* Single-crystal organic heterostructure for single-mode unidirectional whispering-gallery-mode laser. Adv Opt Mater, 2021, 10: 2101931
29 Su Y, Wu B, Chen S, *et al.* Organic branched heterostructures with optical interconnects for photonic barcodes. Angew Chem Int Ed, 2022, 61: e202117857
30 Zhuo MP, He GP, Wang XD, *et al.* Organic superstructure microwires with hierarchical spatial organisation. Nat Commun, 2021, 12: 2252
31 Zhu W, Sun Y, Liu J, *et al.* Exciton transport in molecular semiconductor crystals for spin-optoelectronics paradigm. Chem Eur J, 2021, 27: 222–227
32 Catalano L, Berthaud J, Dushaq G, *et al.* Sequencing and welding of molecular single-crystal optical waveguides. Adv Funct Mater, 2020, 30: 2003443
33 Lu Z, Zhang Y, Liu H, *et al.* Optical waveguiding organic single crystals exhibiting physical and chemical bending features. Angew Chem Int Ed, 2020, 59: 4299–4303
34 Yao W, Yan Y, Xue L, *et al.* Controlling the structures and photonic properties of organic nanomaterials by molecular design. Angew Chem Int Ed, 2013, 52: 8713–8717

Acknowledgements This work was supported by the National Natural Science Foundation of China (21971185 and 52173177), the Collaborative Innovation Centre of Suzhou Nano Science and Technology (CIC-Nano), and the "111" Project of the State Administration of Foreign Experts Affairs of China.

Author contributions Wang XD proposed and guided the overall project. Xu CF fabricated the organic micro-/nanostructures and performed the structural/optical characterization. Lv Q performed the optical testing of microrods. Xu CF, Yang WY, Wang XD, and Liao LS discussed the interpretation of the results and wrote the paper. All authors discussed the results and commented on the manuscript.

Conflict of interest The authors declare that they have no conflict of interest.

Supplementary information Experimental details and supporting data are available in the online version of the paper.

Xue-Dong Wang is a full professor at the Institute of Functional Nano & Soft Materials (FUNSOM), Soochow University. He received his bachelor's degree in chemistry from Lanzhou University in 2011 and his PhD degree in physical chemistry from the Institute of Chemistry, Chinese Academy of Sciences (ICCAS), in 2016. His research focuses on the fine synthesis of organic micro/nanocrystals and organic photonics, including organic solid-state lasers and optical waveguides.

Liang-Sheng Liao received his PhD degree in physics from Nanjing University, China. After working at Eastman Kodak Company as a senior research scientist from 2000 to 2009, he joined FUNSOM, Soochow University, as a full professor. He has over 20 years of research experience in organic optoelectronics. His current research interests include the materials and architectures of organic light-emitting diodes, organic solar cells, and perovskite solar cells.

通过有机晶体定向自组装形成的用于信号处理的芯片状异质结构

许超飞[1†], 杨婉莹[1†], 吕强[1], 王雪东[1*], 廖良生[1,2*]

摘要 有机单晶由于其较低的光传输损耗和可调谐的光学特性，在光限制和光波导领域显示出广阔的应用前景. 单一的一维或二维(1D或2D)光波导晶体在有机光子学中具有单一功能的局限性. 在这项工作中，我们通过精心设计的顺序生长方法制造了一种芯片状的有机异质结构. 通过调节各有机组分的浓度，依次进行溶液自组装、刻蚀和外延自组装过程，完成有机微纳结构的定向生长. 值得注意的是，所制备的芯片状有机异质结构由1D/2D光波导晶体组成，可实现多方向光子传输和多端定向光信号输出. 此外，芯片状异质结构独特的二维光波导特性为构建微/纳米级输出光信号的编码形式提供了机会.

